Amplifying Variability of the Southern Annular Mode in the Past and Future

Ding Ma[1, 2], Yuandong Zhang[1], and Ji Nie[3,4,5*]

1. Division of Natural and Applied Sciences, Duke Kunshan University, Kunshan, Jiangsu, China

2. Environmental Research Center, Duke Kunshan University, Kunshan, Jiangsu, China

3. Laboratory for Climate and Ocean-Atmosphere Studies, Department of Atmospheric and Oceanic Sciences, School of Physics, Peking University, Beijing, China

4. China Meteorological Administration Tornado Key Laboratory, Foshan, China

5. Institute of Carbon Neutrality, Peking University, Beijing, China

Corresponding author address: Ji Nie, Email: jinie@pku.edu.cn

Abstract

The Southern Annular Mode (SAM) is the dominant mode of atmospheric variability in the Southern Hemisphere extratropics. While its long-term positive trend is well-documented, changes in the amplitude of SAM variability remain poorly understood. Based on reanalysis data and surface-station observations, we demonstrate that SAM variability has substantially increased over the past eight decades, coinciding with more frequent and severe weather extremes. A simple model and idealized climate experiments reveal that this amplification is primarily driven by enhanced eddy momentum flux, which is mechanistically linked to a strengthened meridional temperature gradient. State-of-the-art climate model projections under high-emission scenarios indicate that SAM variability will likely continue to intensify throughout the 21st century, driven by a further increase in the meridional temperature gradient. These findings highlight a critical but previously overlooked response of large-scale circulation to climate change, with important implications for assessing and mitigating future climate risks across the Southern Hemisphere.

Significance

The Southern Annular Mode (SAM) is a major driver of weather variability across the Southern Hemisphere extratropics. How the SAM variability will change in the future has significant implications for weather and its impacts: more extremely abnormal SAM event is associated with stronger weather extremes. Here, we demonstrate that SAM variability, along with its associated weather extremes, has significantly intensified over the past eight decades and will continue to amplify under future warming. The mechanism of the amplification as enhanced atmospheric eddy activity driven by a strengthening equator-to-pole temperature gradient. Our findings reveal that increasing SAM variability represents a critical but underappreciated dimension of climate change, with major implications for understanding and predicting future weather extremes in the Southern Hemisphere.

1. Introduction

The Southern Annular Mode (SAM), defined by a dipole of atmospheric pressure anomalies between the mid- and high latitudes of the Southern Hemisphere (SH), represents the leading mode of large-scale atmospheric variability in the SH extratropics (Thompson and Wallace, 2000; Gong and Wang, 1999). Positive (negative) phases of SAM are associated with a poleward (equatorward) shift of the westerly jet (Lorenz and Hartmann, 2001). SAM exerts a profound influence on SH climate and weather, modulating temperature, precipitation, storm activity, and sea ice extent (Gillett et al., 2006; Pezza et al., 2008; Doddridge and Marshall, 2017; Holz et al., 2017). In addition, SAM affects Southern Ocean circulation, biogeochemistry, and carbon uptake (Lovenduski et al., 2007), highlighting its important role in the Earth system. A comprehensive understanding of SAM is therefore critical for interpreting past climate variability and improving projections of future climate change.

Previous studies have consistently documented a robust trend toward the positive phase of the SAM in recent decades (Thompson et al., 2000; Kushner et al., 2001; Marshall, 2003). This shift has been primarily attributed to stratospheric ozone depletion (Thompson et al., 2011). Concurrently, rising greenhouse gas concentrations intensify tropical tropospheric warming and enhance the meridional temperature gradient. This greenhouse-driven effect is expected to sustain the positive SAM trend even as stratospheric ozone recovers in the coming decades (Arblaster and Meehl, 2006; Arblaster et al., 2011). Consistent with these mechanisms, climate simulations from the Coupled Model Intercomparison Project Phase 6 (CMIP6) project a continued shift to the positive SAM phase through the end of the 21st century (Goyal et al., 2021).

However, little research has focused on changes in the variability of the SAM, which may be equally important as shifts in its mean state for regional weather and climate. While a change in the mean SAM state implies a systematic shift in atmospheric circulation—such as displacement of the jet—that can alter weather patterns (Gillett et al., 2006; Pezza et al., 2008), an increase in SAM variability implies more frequent or extreme deviations from the mean, thereby elevating the likelihood of weather extremes. Importantly, similar distinctions between mean and variability responses have been identified in other climate phenomena. For example, the sensitivity of extreme precipitation to global warming is substantially greater than that of mean precipitation (e.g., Seneviratne et al., 2021; Nie et al., 2020). Likewise, the El Niño–Southern Oscillation (ENSO) is projected to exhibit increased variability under climate warming, even though there is no consensus on its mean state changes (Cai et al., 2022; Lee et al., 2022). These examples underscore the critical need to understand not only the mean state response of the SAM, but also potential changes in its variability.

This study quantifies historical and projected changes in SAM variability and investigates the underlying mechanisms. We: (1) present observational evidence for a significant increase in daily SAM variability since the 1940s, accompanied by a corresponding intensification of associated weather extremes; (2) identify the primary drivers of this variability amplification using a simple theoretical model and idealized climate model simulations; and (3) demonstrate that SAM variability is likely to continue increasing under anthropogenic forcing through the end of the 21st century.

These findings underscore that enhanced SAM variability constitutes a critical, yet previously underappreciated, facet of the SH climate response to global change, with important implications for future weather extremes and climate risk assessment.

2. Results

2.1 Historical Amplification of SAM Variability

The historical amplification of SAM variability is clearly evident in the evolving probability distribution of the daily SAM index (z; see Methods), derived from the fifth-generation ECMWF reanalysis (ERA5) beginning in 1940 (Figure 1a). Comparing the periods 1940–1979 and 1980–2019, the distribution shifts toward more positive values, consistent with the well-documented mean-state trend toward a positive SAM phase (e.g., Thompson et al., 2011). Notably, we emphasize the change in the distribution's width—quantified by ±2 standard deviations (vertical dashed lines in Figure 1a)—which expands substantially over time. This widening even dominates the mean shift in its impact on extreme negative SAM events, which become more frequent and intense during the later period despite the overall positive trend. The increase in SAM variability is further confirmed by the year-to-year standard deviation of the daily SAM index (σ_z; Figure 1b), which rises significantly from a mean of 9.61 in 1940–1979 to 10.96 in 1980–2019, representing a 14% increase. Comparable trends are observed in other reanalysis datasets, such as the NCEP reanalysis (Figure S1), supporting the robustness of these findings.

The observed amplification of SAM variability translates directly into more pronounced weather extremes. To illustrate these impacts, we composite anomalies of precipitation, zonal wind, and temperature associated with daily SAM events exceeding ±1 standard deviation (see Methods). Figure 2a presents precipitation anomaly composites averaged over 20°S–40°S—a latitude band selected for consistency with Australian surface observations (Figure S2)—during strong positive SAM events, with longitudes shifted to align regional structures (see Methods). The composites reveal a wave-like precipitation pattern characteristic of synoptic-scale disturbances, with anomaly peaks positioned slightly downstream of the center. Notably, the amplitude of the peak positive precipitation anomaly increases by approximately 0.6 mm day^{-1} between the earlier (1940–1979) and later (1980–2019) periods, corresponding to a 40% fractional increase. These reanalysis-based results are corroborated by Australian surface-station precipitation data (Figure 2b), which exhibit comparable enhancements in precipitation anomalies during positive SAM events.

Further insights into the precipitation patterns are provided by the latitude–longitude composites of SAM-related anomalies (Figure S3). During positive SAM events, strong negative precipitation anomalies are centered around 45°S (absolute latitude) and 0° (relative longitude), flanked by positive anomalies along a northeast–southwest orientation (Figure S3a). In the later period, there is an enhancement of the downstream positive precipitation anomaly (Figure S3b), consistent with the zonal average map (Figure 2). In contrast, negative SAM events are characterized by positive precipitation anomalies located slightly downstream of the composite center (Figure S3c). In the later period, the positive anomalies are more spatially confined and centered around 45°S (Figure S3d). There are negligible changes in the zonally averaged (20°S–40°S) precipitation anomalies between the two periods, as confirmed by both reanalysis and surface data (Figure S4). It is noteworthy that the regional structure and phase asymmetric precipitation response between positive and negative SAM events are consistent with previous studies emphasizing the zonal structure of SAM and its interaction with atmospheric waves (Kushner and Lee, 2007; Luo et al., 2007; Luo et al., 2018).

The amplified variability of the SAM is also evident in other key meteorological variables, including zonal wind and temperature. Composites of vertically averaged zonal wind anomalies during strong SAM events exhibit local meridional dipole patterns (Figures S5a, c), which become more pronounced in the later period due to the increased SAM variability (Figures S5b, d). Similarly, composites of lower-tropospheric temperature anomalies show stronger temperature fluctuations in the later period (Figure S6). In these composites, the long-term trends are removed to isolate the anomalies associated with SAM variability. These results indicate that the amplified SAM variability contributes to substantial and spatially coherent changes in regional wind and temperature patterns, underscoring its broader implications for extreme weather events in the SH.

2.2 Driver of the SAM Variability Amplification

To investigate the dynamical processes underlying the observed amplification of SAM variability, we employ a simple, theoretical model that captures the essential interaction between the SAM and eddy momentum forcing (Lorenz and Hartmann, 2001; see Methods). This model estimates SAM variability given the input of stochastic eddy momentum forcing ($\widetilde{m}$), with parameterized eddy–jet feedback (by a strength parameter b) and damping (by damping timescale τ). Here, we use this model as a diagnostic tool to understand the mechanisms driving changes in SAM variability over time.

We begin by validating the simple model. Using the diagnosed parameters and stochastic eddy momentum forcing from reanalysis, the model reproduces the year-to-year SAM variability (σ_z) with good fidelity (Figure S8a). Notably, both the model parameters (Table S1) and the eddy momentum forcing ($\widetilde{m}$; Figure S7a) differ between the early and later periods. These differences suggest that the observed changes in SAM variability may result from variations in both the parametered processes and the external forcing. To disentangle their respective contributions, we first recompute σ_z using the same parameter values (b and τ) for both periods. The results still exhibit a substantial increase in σ_z after 1979 (Figure S8b). In contrast, when we adjust $\widetilde{m}$ such that its mean is held constant across the two periods (Figure S7b), the amplification in σ_z largely disappears (Figure S8c). These calculations indicate that the increase in SAM variability is primarily driven by enhanced variability in the eddy momentum forcing, rather than by changes in the eddy–jet feedback or damping.

What, then, drives the increase in the variability of eddy momentum forcing? We propose that this enhanced variability arises from a strengthened meridional temperature gradient. As shown in Figure 3a, the 250-hPa temperature difference between 20°S and 70°S—a proxy for the mid-latitude meridional temperature gradient—increases by approximately 1 K from the 1940–1979 period to 1980–2019. Statistical analyses support the following causal pathway: a stronger meridional temperature gradient enhances eddy activity, reflected in increased eddy momentum flux (O'Gorman 2010; Figure S9a), which is associated with greater variability in eddy momentum flux (Figure S9b). This, in turn, drives amplified SAM variability (Figure S9c), as suggested by the simple model. Collectively, these results highlight a positive linkage between the meridional temperature gradient and SAM variability (Figure 3a), providing a physically consistent explanation for the observed amplification.

To further evaluate the proposed mechanism, we conduct a series of idealized experiments using the Geophysical Fluid Dynamics Laboratory (GFDL) dry dynamical core model (Methods). This model excludes moist processes and topographic influences, enabling a focused examination of eddy–mean flow interactions. We systematically vary the prescribed equilibrium meridional temperature gradient across simulations. The results reveal a clear and robust relationship: a stronger meridional temperature gradient leads to increased SAM variability (Figure 3b). The ability of these idealized simulations to reproduce the key features in observations provides strong support for our proposed mechanism, linking the amplification of SAM variability to background climate changes associated with global warming.

2.3 Continuous Increase of SAM Variability in the Future

Having established the historical amplification of SAM variability and its underlying drivers, we now turn to its future projection. To assess how SAM variability may respond to future global warming, we analyze an ensemble of climate simulations from 25 CMIP6 models under the high-emissions scenario SSP5-8.5. These simulations consistently project that SAM variability will continue to increase in a warming climate. Comparing the future period (2060–2099) with a historical baseline (1980–2019), the multi-model mean shows a clear and statistically significant increase in the amplitude of SAM variability by the end of the 21st century (Figure 4). Notably, 19 out of 25 models project a further amplification of SAM variability, although the magnitude of the projected change exhibits sizeable inter-model spread.

All 25 CMIP6 models project an enhancement of the meridional temperature gradient in the SH (Figure 4). This feature is a robust climate response, primarily driven by the delayed warming over the Southern Ocean (Simpkins, 2024). In contrast, the Northern Hemisphere exhibits a weakening meridional temperature gradient due to Arctic amplification (Douville, 2023), and studies suggest that the North Atlantic Oscillation (NAO) may become less variable in a warming climate (Mitevski et al., 2025). These opposing hemispheric responses in both the meridional temperature gradient and annular mode variability are nonetheless consistent with our proposed mechanism. While the majority of CMIP6 models project an increase in SAM variability, six models show a slight weakening despite projecting a stronger meridional temperature gradient. This discrepancy suggests that additional factors may also influence SAM variability in these cases. Possible contributors include changes in the characteristic wavelength of eddies, which can modulate the eddy–jet feedback strength

(Kidston et al., 2010; Dai and Nie, 2020), and biases in the models' climatological states that affect baroclinic instability and eddy dynamics (Chemke et al., 2022).

3. Conclusions and Discussion

This study presents comprehensive evidence for a significant amplification of SAM variability over the past eight decades —an impactful shift in the behavior of the dominant mode of atmospheric variability in the SH extratropics. The enhanced variability is associated with intensified weather anomalies linked to SAM, as confirmed by both reanalysis and surface-station observations. Using a theoretical model and idealized simulations, we identify the primary driver of this amplification as strengthened meridional temperature gradient. Climate projections from CMIP6 models suggest that this amplification of SAM variability is likely to continue through the end of the 21st century under global warming, consistent with the projected intensification of the SH meridional temperature gradient.

Our findings have important implications for future changes in the extreme weather in the SH. The combined effect of a projected increase in SAM variability and a continued positive trend in its mean state is expected to result in more frequent and intense extreme positive SAM events (as illustrated in Figure 1a), along with their associated weather extremes. Moreover, our results reveal phase asymmetry in SAM-associated weather anomalies and their response to variability changes. This is consistent with prior studies that have identified inherent phase asymmetry in the dynamics of annular modes (Luo et al., 2007; Mitevski et al., 2025). This study focuses on projections through the end of the 21st century. Over the time-scale of hundreds of years, as South Ocean warming eventually catches up with the global mean (e.g., Coulon et al. 2024), the SH circulation and SAM behavior may undergo abrupt transitions. Finally, our findings underscore the importance of moving beyond mean-state analysis when evaluating future climate. Variability in large-scale atmospheric modes such as the SAM plays a critical role in shaping regional climate extremes. A comprehensive understanding of both mean and variability changes is essential to provide more interpretable climate projections for policymakers and stakeholders.

Methods

Data. We quantify historical changes in SAM variability from 1940 to 2019 using the fifth-generation European Centre for Medium-Range Weather Forecasts (ECMWF) reanalysis (ERA5; Hersbach et al., 2020). The analysis employs four-times-daily ERA5 data at a horizontal resolution of 1° × 1°. We also utilize the National Centers for Environmental Prediction (NCEP) reanalysis (Kalnay et al., 1996), available at a resolution of 2.5°, spanning 1948–2019. To provide independent observational support, we examine daily in situ measurements from 1,995 Australian surface weather stations (Jones et al., 2009). The stations mostly locate between 20°S and 40°S (Figure S2), aligning with the latitude band used in our composite analyses (Figure 2). Future climate projections are based on daily output from 25 CMIP6 models (Eyring et al., 2016). The high-emission SSP5-8.5 scenario is examined here. In analysis, we remove the climatological seasonal cycle, defined as the annual mean plus the first four Fourier harmonics of the daily climatology, from all datasets. All meteorological fields are subsequently linearly detrended prior to compositing to focus on variability rather than long-term trends.

Definition of the SAM Index. Following established methodologies (e.g., Lorenz and Hartmann, 2001), the SAM index is defined as the principal component time series associated with the leading empirical orthogonal function (EOF) of SH zonal-mean zonal wind anomalies. This definition is applied consistently across all datasets, including reanalysis products, idealized model simulations, and CMIP6 outputs.

Composites. Strong positive and negative SAM events are identified as days when the daily SAM index exceeds ±1 standard deviation. The standard deviation thresholds are calculated separately for the earlier (1940–1979) and later (1980–2019) periods. Composites of precipitation, temperature, and zonal wind anomalies are then constructed based on these anomalous SAM events. Although the SAM is defined as a zonally symmetric mode, the associated weather anomalies often exhibit zonally localized patterns. To identify and align these regional features in the composites, we adopt the local dipole index introduced by Kushner and Lee (2007). This index quantifies longitudinal variations in the jet stream by projecting zonal wind anomalies at each longitude onto the meridional dipole pattern defined by the SAM. When constructing composite maps (e.g., Figures 2, S3), meteorological fields of each event are longitudinally shifted such that 0° relative longitude corresponds to the longitude of the maximum (for positive SAM events) or minimum (for negative SAM events) of the local dipole index. The x-axes in the corresponding composite plots thus represent this shifted (relative) longitude, allowing for consistent alignment of synoptic-scale features across events.

Simple Model. To understand the dynamics underlying the observed increase in SAM variability, we adopt a simple model (Lorenz and Hartmann, 2001), which is written as

$$\frac{dz}{dt} = m - \frac{z}{\tau}, \quad (1)$$

where z is the SAM index, m is the total eddy momentum forcing, and τ the damping timescale. Equation 1 is the governing equation of zonal momentum (i.e., the SAM index) under the eddy momentum forcing and damping. The eddy momentum forcing is written as

$$m = \widetilde{m} + bz, \quad (2)$$

where $\widetilde{m}$ is the stochastic eddy momentum forcing that is externally specified as inputs of the model. bz represents the eddy-jet feedback, with feedback strength of b. The parameters τ and b are treated as constants, at least for a certain time period. The input, $\widetilde{m}$, allows annual variability. Here we use the simple model as a tool to understand the changes in SAM variability. Thus, the parameters (τ and b) and model input ($\widetilde{m}$) are not prescribed a priori, but diagnosed from the reanalysis following the method in Lorenz and Hartmann (2001). With diagnosed b, τ (Table S1), and $\widetilde{m}$ (Figure S7a), the simple model can reproduce the observed SAM variability very well

(Figure S8a), indicating its capability in explaining the changes in SAM variability.

Idealized Climate Experiments. Numerical experiments were conducted using the Geophysical Fluid Dynamics Laboratory (GFDL) dry dynamical core model. This idealized model excludes moisture processes and represents surface conditions using a homogeneous lower boundary with no topography. Radiation is simplified as a relaxation of atmospheric temperature toward a prescribed, zonally symmetric radiative equilibrium temperature profile, with equator-to-pole surface temperature difference (ΔT_y ;Held and Suarez, 1994). This modeling configuration has been widely used to investigate eddy–jet feedbacks and annular mode dynamics (e.g., Ma et al., 2017). To explore the link between meridional temperature gradients and SAM variability, we perform a suite of simulations in which ΔT_y is systematically varied from 45 K to 70 K in 5 K increments. Each simulation is integrated for 15,600 model days at T63 horizontal resolution (approximately 200 km grid spacing), with 40 vertical levels and 6-hourly output. The initial 1,000 days are discarded as spin-up, and the remaining 40 years of data are used for analysis. Owing to the model's hemispheric symmetry, each simulation effectively provides 80 years of annular mode data.

Acknowledgments

This work is supported by Jiangsu Natural Science Foundation Grant BK20241828 (to D.M.), National Key R&D Program of China grant 2023YFF0805200 and National

Natural Science Foundation of China 42375057 (to J.N.).

Author contributions

D.M. and J.N. designed and performed the study. D.M. and Y.Z. conducted data analysis. D.M. and J.N. wrote the paper with contributions from Y.Z.

Competing interests

The authors declare no competing interests.

Materials & Correspondence

Correspondence and requests for materials should be addressed to J.N.

Data availability

The ERA5 reanalysis is available at https://cds.climate.copernicus.eu/datasets/reanalysis-era5-pressure-levels. The surface-station observational data are provided by the Australian Bureau of Meteorology at http://www.bom.gov.au/climate/data/. The CMIP6 climate simulation dataset is available at https://esgf-node.llnl.gov/search/cmip6/. The analyses data in the paper will be made available after the first round of review.

References

Arblaster J, Meehl G (2006) Contributions of External Forcings to Southern Annular Mode Trends. *Journal of Climate 19*:2896–2905.

Arblaster J, Meehl G, Karoly D (2011) Future Climate Change in the Southern Hemisphere: Competing Effects of Ozone and Greenhouse Gases. *Geophysical Research Letters 3*8(2):L02701.

Cai, W, et al. (2022) Increased ENSO Sea Surface Temperature Variability Under Four IPCC Emission Scenarios. *Nature Climate Change 12*:228–231.

Chemke R, Ming Y, Yuval J (2022) The Intensification of Winter Mid-Latitude Storm Tracks in the Southern Hemisphere. *Nature Climate Change 12*(6):553–557.

Coulon, V, et al. (2024) Disentangling the Drivers of Future Antarctic Ice Loss with a Historically Calibrated Ice-Sheet Model. *The Cryosphere 18*:653–681.

Dai P, Nie J (2022) Robust Expansion of Extreme Midlatitude Storms under Global Warming. *Geophysical Research Letters 49*:e2022GL099007.

Doddridge E, Marshall J (2017) Modulation of the Seasonal Cycle of Antarctic Sea Ice Extent related to the Southern Annular Mode. *Geophysical Research Letters 44*(19):9761–9768.

Douville, H (2023) Robust and Perfectible Constraints on Human-Induced Arctic Amplification. *Communications Earth and Environment 4*(1):283.

Eyring V, et al. (2016) Overview of the Coupled Model Intercomparison Project Phase 6 (CMIP6) Experimental Design and Organization. *Geoscientific Model Development 9*(5):1937–1958.

Gillett N, Kell T, Jones P (2006) Regional Climate Impacts of the Southern Annular Mode. *Geophysical Research Letters 33*(23):L23704.

Gong D, Wang S (1999) Definition of Antarctic Oscillation Index. *Geophysical Research Letters 26*(4):459–462.

Goyal, R., et al. (2021) Historical and Projected Changes in the Southern Hemisphere Surface Westerlies. *Geophysical Research Letters 48*(4):2020GL090849.

Held I, Suarez M (1994) A Proposal for the Intercomparison of the Dynamical Cores of Atmospheric General Circulation Models. *Bulletin of the American Meteorological Society 75*:1825–1830.

Hersbach H, et al. (2020) The ERA5 Global Reanalysis. *Quarterly Journal of the Royal Meteorological Society 146*(730):1999–2049.

Holz A, et al. (2017) Southern Annular Mode Drives Multicentury Wildfire Activity in Southern South America. *Proceedings of the National Academy of Sciences 114*(36):9552–9557.

Jones D, Wang W, Fawcett R (2009) High-quality Spatial Climate Data-Sets for Australia. *Australian Meteorological and Oceanographic 59*:233–248.

Kalnay E, et al. (1996) The NCEP/NCAR 40-Year Reanalysis Project. *Bulletin of the American Meteorological Society 77*:437–471.

Kidston J, et al. (2010) A Robust Increase in the Eddy Length Scale in the Simulation of Future Climates. *Geophysical Research Letters, 37*(3):L03806.

Kushner P, Lee G (2007) Resolving the Regional Signature of the Annular Modes. *Journal of Climate 20*(12):2840–2852.

Kushner P, Held I, Del Worth T (2001) Southern Hemisphere Atmospheric Circulation Response to Global Warming. *Journal of Climate 14*:2238–2249.

Lee, S, et al. (2022) On the Future Zonal Contrasts of Equatorial Pacific Climate: Perspectives from Observations, Simulations, and Theories. *npj Climate and Atmospheric Science 5*(1):82.

Lorenz D, Hartmann D (2001) Eddy-Zonal Flow Feedback in the Southern Hemisphere. *Journal of the Atmospheric Sciences 58*(21):3312–3327.

Lovenduski N, Gruber N, Doney S, Lima I (2007) Enhanced CO2 Outgassing in the Southern Ocean from a Positive Phase of the Southern Annular Mode. *Global Biogeochemical Cycles 21*(2):GB2026.

Luo D, Chen X, Feldstein S (2018) Linear and Nonlinear Dynamics of North Atlantic Oscillations: A New Thinking of Symmetry Breaking. *Journal of the Atmospheric Sciences 75*(6):1955–1977.

Luo D, Lupo A, Wan H (2007) Dynamics of Eddy-Driven Low-Frequency Dipole Modes. Part I: A Simple Model of North Atlantic Oscillations. *Journal of the Atmospheric Sciences 64*:3–28.

Ma D, Hassanzadeh P, Kuang Z (2017) Quantifying the Eddy-Jet Feedback Strength of the Annular Mode in an Idealized GCM and Reanalysis Data. *Journal of the Atmospheric Sciences 74*:393–4.

Marshall G (2003) Trends in the Southern Annular Mode from Observations and Reanalyses. *Journal of Climate 16*(24):4134–4143.

Mitevski, I, et al. (2025) More Positive and Less Variable North Atlantic Oscillation at High CO2 Forcing. *npj Climate and Atmospheric Science 8*:171.

Nie J, Dai P, and Sobel A (2020) Dry and Moist Dynamics Shape Regional Patterns of Extreme Precipitation Sensitivity. *Proceedings of the National Academy of Sciences 117*:8757-8763.

O'Gorman, P. (2010) Understanding the Varied Response of the Extratropical Storm Tracks to Climate Change. *Proceedings of the National Academy of Sciences 117*: 19176–19180.

Pezza A, Durrant T, Simmonds I (2008) Southern Hemisphere Synoptic Behavior in Extreme Phases of SAM, ENSO, Sea Ice Extent, and Southern Australia Rainfall. *Journal of Climate 21*:5566–5584.

Seneviratne S, et al. (2021) Weather and Climate Extreme Events in a Changing Climate. In *IPCC Climate Change 2021: The Physical Science Basis*. Cambridge University Press, Cambridge, United Kingdom and New York, NY, USA, pp. 1513–1766.

Simpkins, G. (2024) Drivers of Southern Ocean cooling. *Nature Review Earth and Environment 5*(1):4.

Thompson D, et al. (2011) Signatures of the Antarctic Ozone Hole in Southern Hemisphere Surface Climate Change. *Nature Geoscience 4*(11):741–749.

Thompson D, Wallace J (2000) Annular Mode in the Extratropical Circulation. Part I Month-to-Month Variability. *Journal of Climate 13*(5):1000–1016.

Thompson D, Wallace J, Hegerl G (2000) Annular Modes in the Extratropical Circulation. Part II Trends. *Journal of Climate 13*(5):1018–1036

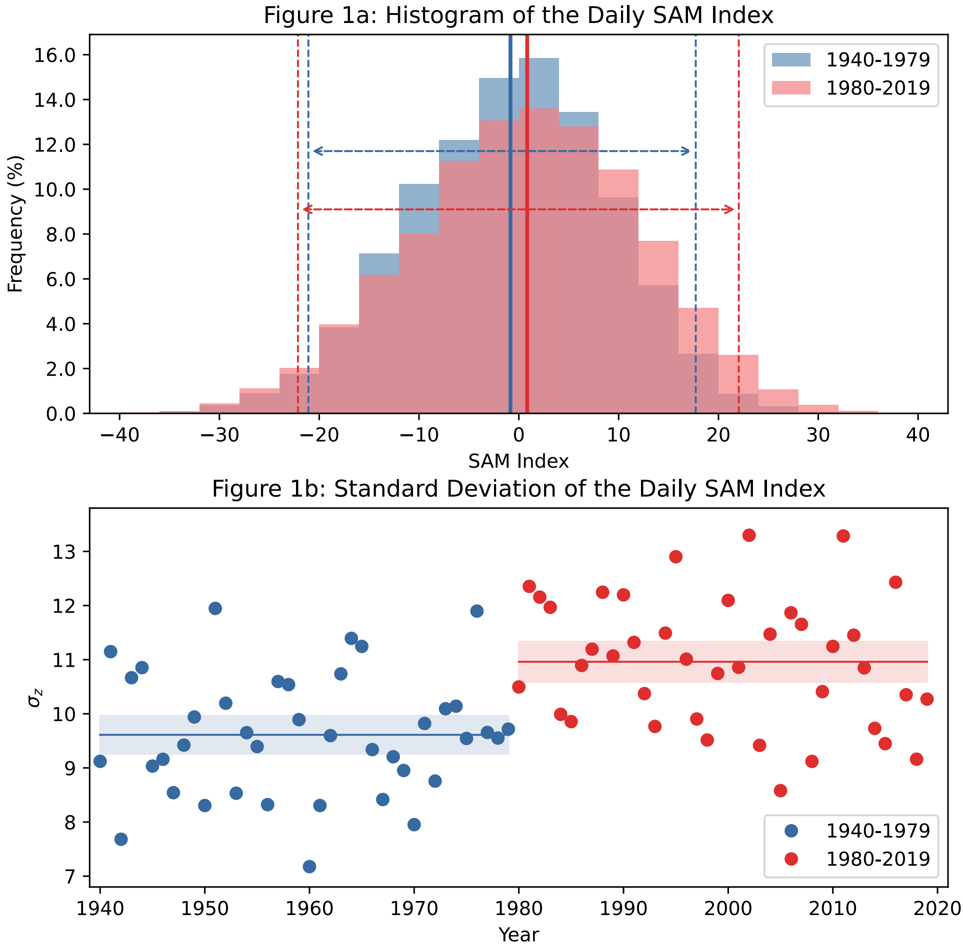

Figure 1. SAM variability from ERA5 data. (a) Histograms of daily SAM index distributions for the historical periods 1940–1979 (blue) and 1980–2019 (red). Solid vertical lines indicate the period means, while dashed lines denote ±2 standard deviations. (b) Annual standard deviation of the daily SAM index over 1940–2019. Horizontal lines show the mean values for each period, and shading represents the 95% confidence interval.

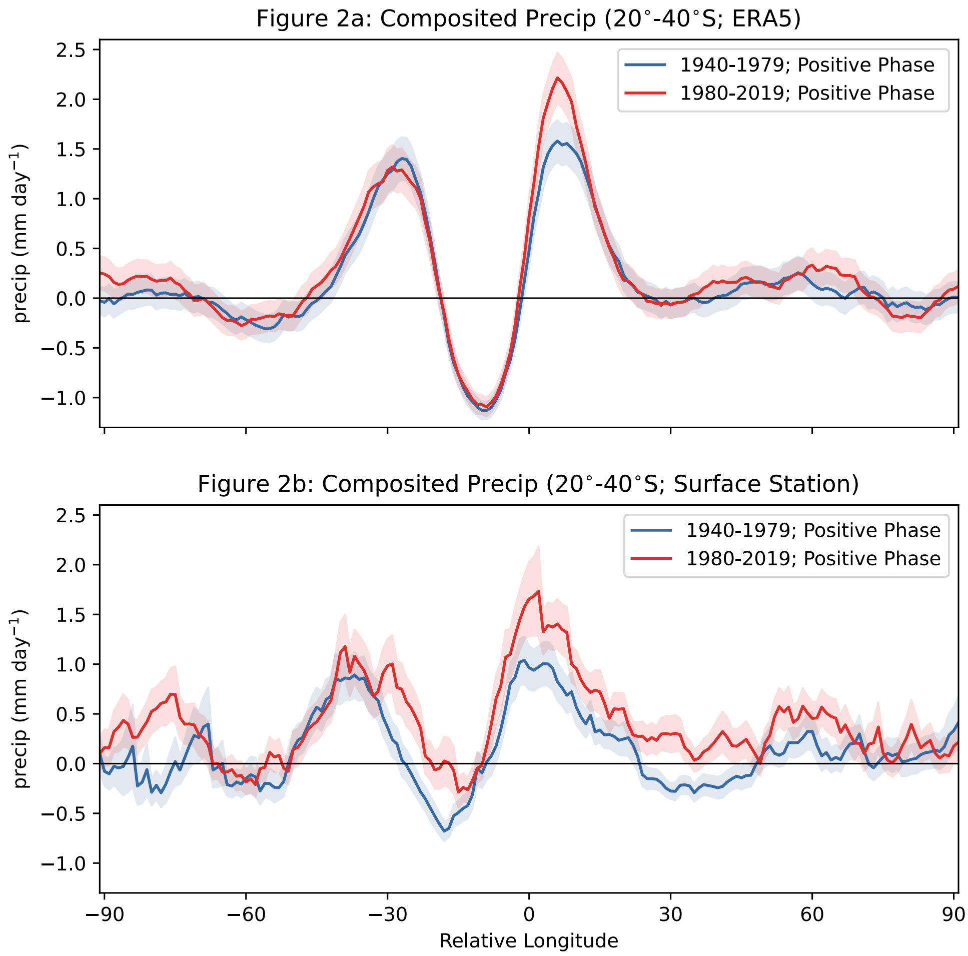

Figure 2. Composited precipitation anomalies (mm day^{-1}) averaged over 20° S – 40°S during strong positive SAM events. (a) ERA5 reanalysis and (b) Australian surface station observations for the periods 1940–1979 (blue) and 1980–2019 (orange). Shading indicates the 95% confidence interval. Note that the x-axis represents relative longitude, aligned to emphasize regional structures (Methods).

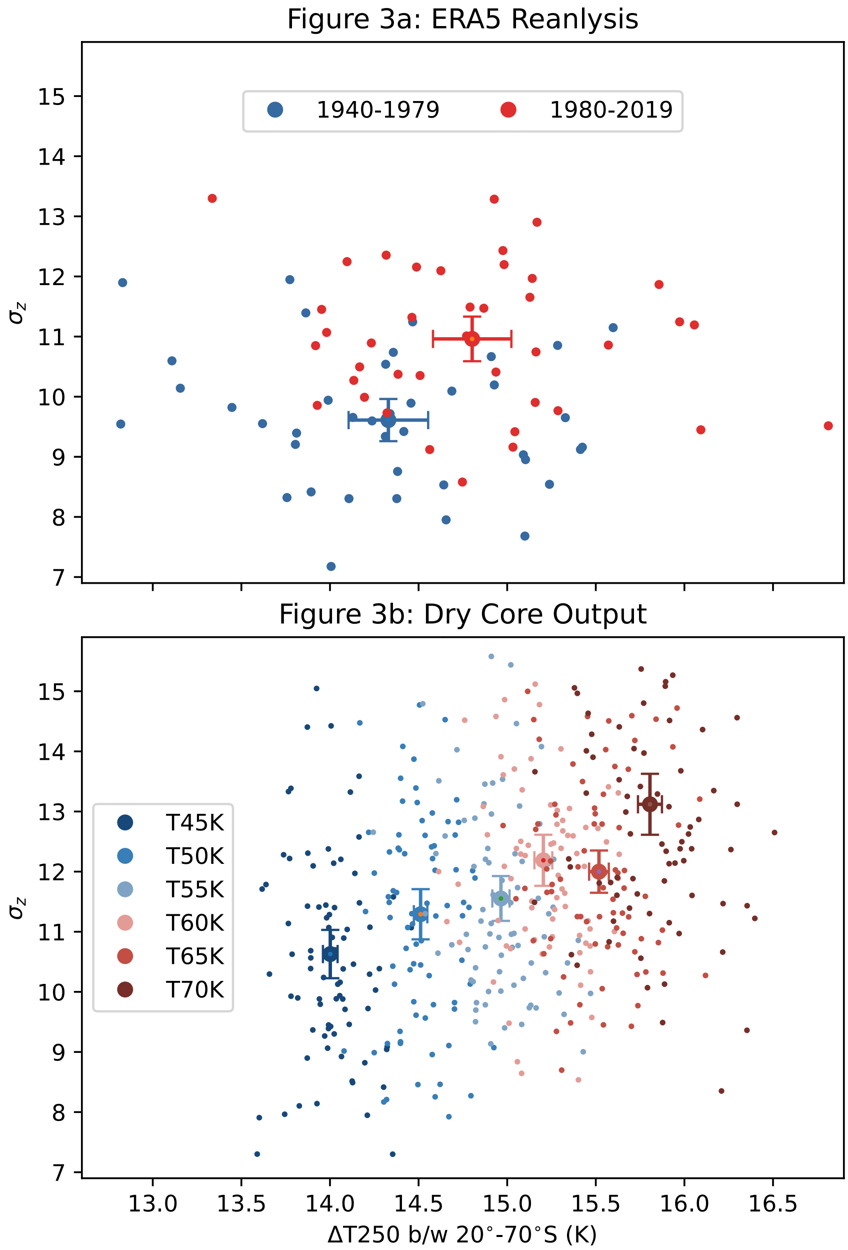

Figure 3. Relationship between SAM variability and meridional temperature difference. (a) is from the ERA5 reanalysis and (b) is from the simulations using the dry dynamical core model. The x-axis is the 250-hPa temperature difference between 20°S and 70°S, and the y-axis shows SAM variability. In (a), colors indicate different time period, and each dot denotes results of one year. In (b), colors indicate different experimental group, and each dot denotes results of one model year. The group means with their 95% confidence intervals are also shown.

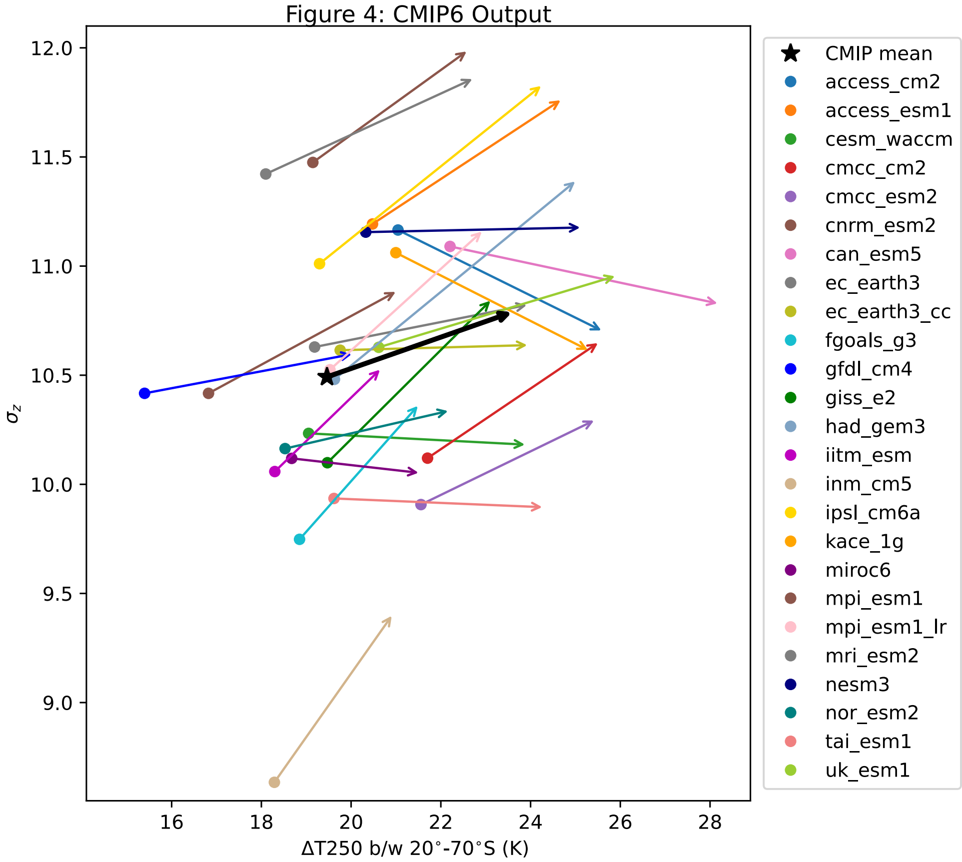

Figure 4. Changes in SAM variability and meridional temperature difference in CMIP6 simulations. Each arrow represents an individual CMIP6 model (identified in the legend), with the starting and ending points indicating the period means for 1980–2019 and 2060–2099, respectively. The multi-model mean is shown as a bold black arrow.